Title

Nose-to-brain transport of aerosolised quantum dots following acute exposure

Journal

Nanotoxicology, 8(8)

ISSN

1743-5390

Authors

Hopkins, Laurie E

Patchin, Esther S

Chiu, Po-Lin

et al.

Publication Date

2014-12-01

DOI

10.3109/17435390.2013.842267

Peer reviewed

Published in final edited form as:
Nanotoxicology. 2014 December ; 8(8): 885–893. doi:10.3109/17435390.2013.842267.

Nose-to-Brain Transport of Aerosolized Quantum Dots Following Acute Exposure

Laurie E. Hopkins[1,*], **Esther S. Patchin**[1,*], **Po-Lin Chiu**[2], **Christina Brandenberger**[3], **Suzette Smiley-Jewell**[1], and **Kent E. Pinkerton**[1]

[1]Center for Health and the Environment, University of California, One Shields Ave., Davis, CA 95616 [2]Molecular and Cellular Biology, One Shields Ave., Davis, CA 95616 [3]Institute of Anatomy, University of Bern, Bern, Switzerland

Abstract

Nanoparticles are of wide interest due to their potential use for diverse commercial applications. Quantum dots are semiconductor nanocrystals possessing unique optical and electrical properties. Although quantum dots are commonly made of cadmium, a metal known to have neurological effects, potential transport of quantum dots directly to the brain has not been assessed. This study evaluated whether quantum dots (CdSe/ZnS nanocrystals) could be transported from the olfactory tract to the brain via inhalation. Adult C57BL/6 mice were exposed to an aerosol of quantum dots for one hour via nasal inhalation, and nanoparticles were detected three hours post-exposure within the olfactory tract and olfactory bulb by a wide range of techniques, including visualization via fluorescent and transmission electron microscopy. We conclude that following short-term inhalation of solid quantum dot nanoparticles, there is rapid olfactory uptake and axonal transport to the brain/olfactory bulb with observed activation of microglial cells, indicating a pro-inflammatory response. To our knowledge, this is the first study to clearly demonstrate that quantum dots can be rapidly transported from the nose to the brain by olfactory uptake via axonal transport following inhalation.

Keywords

qdots; olfactory epithelium; olfactory bulb; inhalation

INTRODUCTION

Quantum dots (QD) are semiconductor nanocrystals that are generally within the size range of ~2 – 100 nm. They offer unique optical and electrical properties, such as bright photoluminescence, narrow fluorescence emission bands, broad UV excitation, “size-tunable” fluorescence, and high resistance to photobleaching and photostability (Ballou et al. 2004, Chang et al. 2006, Hardman 2006, Rzigalinski and Strobl 2009). QD are currently being researched for various uses, such as biological imaging for DNA hybridization

*Both authors contributed equally to the preparation and performance of this research.

detection, immunoassays, binding assays using fluorescence resonant energy transfer (FRET) to probe for target events, cancer detection and treatment, radio- and chemo sensitizing agents and targeted drug delivery (Bailey et al. 2004, Rzigalinski and Strobl 2009). QD can be made with a variety of metals, but cadmium (Cd) and selenium (Se) are two of the most widely used constituent metals in QD core metalloid complexes with fluorescence spanning the visible light region of the spectrum (Hardman 2006, Rzigalinski and Strobl 2009). However, since Cd is a known carcinogen and is associated with liver and kidney injury, osteomalacia, osteoporosis, skeletal deformations, neurological and other deficits, zinc sulfide (ZnS), another semiconductor, is grown over the CdSe core (Hines and Guyot-Sionnest 1996, Rzigalinski and Strobl 2009). ZnS enhances fluorescence efficiency, reduces the toxicity imparted by the highly reactive Cd core, increases chemical stability and makes QD less prone to oxidation and photobleaching (Rzigalinski and Strobl 2009).

As ever-increasing biotechnology applications use QD, the risk of occupational exposure to QD during manufacturing and handling of QD preparations will rise (Hardman 2006, Rzigalinski and Strobl 2009). Inhalation is an important route of exposure because not only can nanoparticles (particles that are < 100 nm in any one dimension) reach the circulation from the lungs, but they can also potentially reach the brain via the olfactory nerves. The anatomy of the olfactory system puts the central nervous system in direct contact with the external environment via olfactory nerves, a cranial nerve, connecting olfactory epithelium to the olfactory bulb in the CNS (Fig. 1) (Kovacs 2004). Previous studies of solid nanosized particles, such as silver-coated gold colloids, have been shown to translocate along the olfactory nerve axons. Elemental carbon particles (^{13}C; 35 nm) have also been shown to accumulate in rat olfactory bulb after whole body inhalation (Aschner 2009, De Lorenzo 1970, Elder et al. 2006, Oberdorster et al. 2004). Recently, Patel et al. (2011) confirmed the presence of risperidone (an antipsychotic medication) in the mouse brain by gamma scintigraphy following intranasal administration of risperidone-loaded solid lipid nanoparticles. These studies demonstrate an end result of nose to brain transport of solid nanoparticles that indicate the potential for other nanoparticles, such as QD, to transport to the brain by the same pathway following inhalation.

To the best of our knowledge, QD transport from nose to brain after inhalation exposure as well as deposition and toxicity have not been well studied. Thus, the primary objective of the present study was to determine (1) if QD reach the olfactory bulb by axonal transport (within olfactory sensory nerves) following inhalation exposure and (2) if QD made of CdSe/ZnS elicits an effect within the olfactory bulb. We present results from a series of experiments in which mice were exposed to aerosols of CdSe/ZnS QD and their olfactory tissues examined for evidence of particle uptake and transport. Since Cd and particulate matter are known to induce oxidative stress, microglial activation was assessed to determine QD responses within the olfactory bulb. Results provide conclusive evidence of QD broadly dispersed in olfactory nerve axons and the olfactory bulb with an induced pro-inflammatory response after inhalation.

MATERIALS AND METHODS

Animals

Adult C57BL/6 mice weighing 25–30 g were purchased from Charles Rivers Labs. Upon arrival, mice were randomly assigned to two treatment groups, QD (n=6) or sham (QD-free, polyethylene glycol phosphatidyl ethanolamine suspension) (n=6) for a total of 12 animals per tissue process, and allowed to acclimate for at least one week prior to the onset of experimental exposures. Mice were housed, up to four per cage, in filter-top polycarbonate cages in an animal facility with high-efficiency particulate air filters. Except during actual exposure periods, mice were allowed water and a standard laboratory diet (Rodent Laboratory Diet code # 5001, Lab Diet) *ad libitum*. Care was taken to ensure animals were handled in accordance with the Guide for the Care and Use of Laboratory Animals and conducted under an animal use protocol approved by the Institutional Animal Care and Use Committee of the University of California, Davis.

Particle Generation

Non-functionalized CdSe/ZnS core-shell QD (EviDots, Evident Technologies, Troy, NY) with a core size of 1.9 nm were encapsulated in polyethylene glycol phosphatidyl ethanolamine (PEG2-PE, PEG2000-PE, MW 2749, Avanti Polar Lipids, Alabaster, AL). PEG2-PE is a micelle-forming hydrophilic polymer-grafted lipid with many advantages, such as consistency in size, shape and structure; de-agglomeration of particles; improvement of particle solubility as well as poor immunogenicity/antigenicity to increase biodistribution and retention time of particles (Dubertret et al. 2002). Encapsulation of QD followed the method described in Dubertret et al. (2002), with slight modification (Fig. 2). Briefly, small volumes of QD in toluene and PEG2-PE in chloroform were combined with PEG2-PE in excess in a glass dish. Following removal of solvents by evaporation, the resulting film was heated temporarily in a water bath to 70° C, at which point double-distilled water was added with gentle agitation to yield a QD solution. This technique yields an optically clear aqueous suspension of self-assembling PEG2-PE micelles, each containing no more than a few individual QD trapped within the interior. Dubertret et al. (2002) reported that encapsulation of QD in PEG2-PE micelles increases their overall diameter to ~15 nm. Exposure with heat was minimized to avoid fluorescence quenching, as reported in the literature (Alivisatos et al. 2005).

Aerosol inhalation exposures

Animals were exposed by a nose-only inhalation system via a continuous low flow nebulizer (MiniHEART, Westmed Inc., Tucson, AZ) to either a QD-free PEG2-PE micelle suspension or an aqueous suspension of PEG2-PE encapsulated QD for a single, acute one hour exposure period.

Aerosol generation and characterization

Samples of the QD aerosol were characterized and visualized by several methods to determine whether encapsulation affected the fluorescent properties of the QD or

aerosolization had any major deleterious effects on the encapsulation, such as dismantling of micelles or the merging of smaller micelles into larger micelles.

Spectrophotometric characterization—A Cary Eclipse fluorescence-capable spectrophotometer (Varian, Inc., Palo Alto, CA) was used to analyze an aliquot of each QD suspension before and after aerosolization to determine if nebulization adversely affected the PEG2-PE micelles or otherwise interfered with QD luminescence.

Droplet sizing characterization—A scanning mobility-based particle sizing system (SMPS #3936, TSI Inc., Shoreview, MN) sampled the aerosol for 135 seconds at 10 minute intervals, beginning from the initiation of nebulization to obtain droplet size distribution data and to determine whether the QD aerosol was delivered consistently during each exposure period. Average aerosol size (nm) was represented by cluster size of QD micelles observed by transmission electron microscopy (Raabe et al. 1998). The distribution of droplet size over time via SMPS measurements was used to determine whether QD concentration was reasonably constant during the exposure period. A cascade impactor was also implemented to collect samples of different sizes generated by the nebulizer at each impactor stage to determine the agglomerate size distribution in the aerosol. The mass median aerodynamic diameter (MMAD) (μm) was determined for clusters of QD micelles captured within an agglomerated droplet. Measurements were calculated from mass determinations for each of the different stages of the cascade impactor.

Aerosol characterization at the animal breathing zone—To verify that particles would remain suspended in the air stream and travel through the entire exposure inhalation system rather than only coating interior surfaces, Teflon-coated Pallflex glass filters (Ted Pella Inc., Redding, CA) were placed in nose ports and the outlet air path for one hour while the system was operating. Exposed filters were examined by fluorescent light microscopy.

Necropsy and tissue collection

At a post-exposure period of 3 hours, all groups of mice were anesthetized by intraperitoneal injection of sodium pentobarbital at 1 mg/kg body weight and euthanized via exsanguination in association with either systemic perfusion with Karnovsky's solution (for transmission electron microscopy) or 4% paraformaldehyde (for immunohistochemistry). Olfactory bulbs were collected from all animals. For a subset of animals, nasal lavage and olfactory bulbs were immediately collected and processed rather than fixed for QD detection.

Recovery of quantum dots by nasal lavage

Heads were removed immediately after death, followed by nasal lavage collection (n=6 QD exposed, n=6 sham). Nasal lavage was collected at the nares via retrograde flush of the nasal cavity with a total volume of 1 mL Hank's Balanced Salts Solution (HBSS) per animal introduced to the exposed tracheolarynx and nasopharyngeal choanae. Nasal lavage fluid (NLF) was centrifuged at 14,000 rpm for 10 minutes. Both fractions, supernatant and re-suspended pellet, were analyzed by fluorescence spectrometry and visualized by fluorescent light microscopy.

Preparation of tissue lysates

Immediately after nasal lavage collection, unfixed, non-perfused olfactory bulbs were collected for QD detection and processed immediately for spectrophotometry (n=6 QD exposed, n=6 sham). Tissue samples were enzymatically digested at 37° C in a 1 mg/mL ProteinaseK solution containing magnesium chloride and calcium chloride at pH 7.8 for four hours. ProteinaseK solution was used in sufficient volume to achieve a 5:1 fluid volume to tissue weight ratio. Lysates were centrifuged at 14,000 rpm for 10 minutes. Supernatant and re-suspended pelleted fractions in room temperature HBSS, were transferred to black 96-well plates (200 μL/well), excited at 360 nm, and read at 5 nm increments between 420 to 700 nm using a CARY Eclipse spectrophotometer (Varian, Inc., Palo Alto, CA).

Preparation of tissue sections

A number of different approaches were used to prepare nasal and olfactory bulb tissues for histological visualization. Fixation in all instances was achieved by vascular perfusion with heparinized phosphate buffer solution (PBS) followed by fixative (n=6 QD exposed, n=6 sham for each preparation): 1) 4% paraformaldehyde for paraffin-embedded tissues for fluorescence energy loss detection and microglial activation, 2) 2% glutaraldehyde in cacodylate buffer for Spurr's resin and electron microscopy, 3) 4% paraformaldehyde and methacrylate-embedded tissues for QD detection and 4) cryosections (olfactory bulb only) for QD detection. Bony nasal tissues were decalcified in 0.5 M EDTA at pH 8.0 for at least one week prior to embedment. Paraffin sections were cut by microtome to a thickness of 5 μm and mounted on glass slides. Methacrylate sections were cut to a thickness of 2 μm. Cryosections of olfactory bulbs were cut to a thickness of 10 μm. For electron microscopy, perfusion-fixed tissues were trimmed, post-fixed by immersion in osmium tetroxide solution, dehydrated and embedded in Spurr's resin. Silver-gold sections (~70 nm thick) were cut by an ultramicrotome and mounted on 400 mesh copper grids coated with Type B carbon support film (#01814-F, Ted Pella, Inc., Redding, CA). Half of the sections were stained with uranyl acetate, while the remaining sections were left unstained.

Visualization of quantum dots in mice

QD were visualized in tissue sections by fluorescent light microscopy and transmission electron microscopy (TEM) by individuals blinded to the treatment groups. Luminance profiles (expressed in ALU) were measured in olfactory bulb tissue lysates at a wavelength of 490 nm corresponding with known emission peak (of 490 nm) of the QD suspension. QD emission peaks were read by the spectrophotometer with the center (nm at maxima) and breadth of peak identified and compared.

Fluorescent light microscopy—Monochrome images were captured using an Olympus BH-61 upright microscope equipped with 100 Watt mercury lamp, Chroma 88000 filter set, and SPOT RT3 digital camera. Color images were captured using a Zeiss Axiovert 40CFL inverted microscope with an Xcite light source, Zeiss 02 filter set, and SPOT5 color digital camera. False color images were captured using an inverted Olympus IX-71 microscope with an Innova 70C Arkr ion gas laser (Coherent, Santa Clara, CA), an Andor acusto-optic tunable filter and an iXon 897 EM-CCD camera.

Transmission electron microscopy—Samples of the aerosol, captured by electrostatic precipitation, and thin sections of resin-embedded tissue were imaged using a JEOL JEM-2100 TEG/STEM electron microscope equipped with 4k CCD camera. Uranyl acetate was applied to tissue sections to improve contrast, although the staining imparts some granularity to the images. The lack of sharp contrast in our TEM images of tissue sections was in large part due to the fact that type-B 'heavy' carbon support film (15–25 nm thick) on all copper mesh and oval grids was necessary.

Microglial cell visualization and counts

Ricinus communis agglutinin lectin (RCA-1, Vector Labs, Burlingame, CA) histochemical staining, after the technique of Hauke and Korr with modification (1993), was used to visualize microglial cells in paraffin sections of the glomerular layer of the olfactory bulb. Briefly, tissue sections were deparaffinized, incubated with RCA-1 followed by diaminobenzidine chromogen plus substrate (Dako North America, Carpinteria, CA) for visualization, counterstained with hematoxylin and mounted.

Although RCA-1 binds to β–D-galactose moieties present on microglial, epithelial and vascular endothelial cells, all three types of cells can be easily differentiated on the basis of their morphology. Microglial cells were counted in six fields per histological section, two sections per animal, and six animals per exposure group at a magnification of 400x (using a 40x objective lens with a 10x projection eyepiece) on a BH2 Olympus microscope. Every qualifying microglial cell was counted in each of six randomly selected non-overlapping fields per section by employing a zigzag pattern for field sampling. Microglial cells were classified as either resting or activated using pre-determined criteria based on Stence's characterization of ramified (resting) versus motile (activated) stages (Stence et al. 2001). Microglial cells exhibit a range of morphological conformations correlating with activation state, presenting a gradient from resting to fully activated (Colton and Wilcock 2010, Lawson et al. 1990, Stence et al. 2001). Resting microglial cells were characterized as having ramified processes whereas activated microglial cells had an enlarged cell body with several short, thickened processes (Stence et al. 2001). Microglial cells per category were summed for each animal, and exposure group means were calculated. Group means for total and category counts were compared to identify exposure-related changes. Increased total number of microglial cells was considered a measure of recruitment. RCA-1 positive cells not meeting either set of criteria (i.e., intermediate forms) were excluded. All histological examinations were done in a blinded fashion.

Statistics

JMP version 10.0.0 (Cary, NC) and GraphPad Prism version 3.00 (San Diego, CA) statistical software were used to perform Gaussian tests of normality, Levene and Bartlett's test for homoscedasticity, and/or Student's t-test with a significance level of $p \leq 0.05$. The tests demonstrated both normality and homoscedasticity of the data used for statistical analysis.

RESULTS

Aerosol inhalation exposures

Aerosolized QD maintained their PEG2-PE encapsulated micelle with a total diameter of 15–20 nm with a QD core diameter of 1.9 nm. Spectrophotometry data revealed that the spectra and fluorescence intensity at an emission peak wavelength of 490 nm (blue) did not diminish with aerosolization or time of exposure. If QD shell/core were degraded, fluorescence would not have been observed. Supporting the spectrophotometry data, TEM images of aerosol droplets captured by electrostatic precipitation onto EM copper mesh grids demonstrated that the PEG2-PE micelles containing QD were not dismantled by aerosolization. Individual micelles appeared as dark QD cores, each surrounded by an electron lucent halo composed by the PEG2-PE, which forms the micelle (Fig. 3).

Droplet sizing

Scanning mobility-based particle sizing data for PEG2-PE encapsulated QD aerosols were generated on five separate occasions. Droplet size distribution and mass concentration remained consistent for each sample over the one hour exposure period with an average particle diameter of ~84 nm and an average concentration of 250 $\mu g/m^3$. The mass median aerodynamic diameter (MMAD), obtained from serial stages of the cascade impactor, was utilized to yield an agglomerate size in the aerosol of 1.8 μm with a geometric standard deviation (sigma g) of 2.24.

Nasal delivery

Filters placed in the aerosol outlet and the sampling ports during exposure were moist at removal, confirming that the aerosol droplets did not evaporate during transport from the nebulizer to the nose ports of the inhalation system and that the mice were inhaling suspension droplets containing encapsulated QD. Under fluorescent light microscopy, the filters exhibited copious intense fluorescence consistent with the QD forms used in the study.

Recovery of inhaled quantum dots by nasal lavage

QD recovered three hours post-exposure by retrograde flush of the nasal cavity were found in readily detectable amounts. Under excitation by UV light, supernatant and re-suspended pellets from nasal lavage fluid exhibited bright fluorescence at emission peak wavelength of 490 nm (blue), corresponding to the 1.9 nm diameter core QD in the aerosol. Total fluorescence in the QD-exposed group was 37% above background (8310 arbitrary light units (ALU) vs. 6060 ALU in shams).

Detection of quantum dots in tissue

Tissue lysates—Analysis of olfactory bulb tissue digests with fluorescent light microscopy revealed the presence of QD (1.9 nm cores, blue) in the QD-exposed group but not in the shams (Fig. 4). A quantitative technique, fluorospectrophotometry showed total fluorescence (as evidenced by QDs' characteristic emission wavelength) in the QD-exposed group was 26% above background (57365 ALU vs. 45355 ALU in shams). This data

conclusively demonstrates that detectable numbers of QD reached the olfactory bulbs within three hours post-exposure of a single one-hour inhalation exposure.

Tissue sections—Investigation of tissue embedded in resin sections with fluorescent light microscopy clearly showed multiple foci of QD color inside cells of the glomerular layer. QD appeared as high-intensity punctate luminance in the cytoplasm but not in the nucleus (Fig. 5). There was no evidence of QD in deeper layers of the olfactory bulb, and QD were only rarely observed within the olfactory epithelium, where they were in close association with olfactory neurons.

Visualization of paraffin-embedded tissue sections of the nasal cavity, nerves fascicles and olfactory bulb by energy loss fluorescence detection demonstrated a low level of diffuse excitation energy loss within the nerve fascicles passing through the cribiform plate (Fig 6). Cryosections of the olfactory bulb also demonstrated the clear aggregation of fluorescent clustering indicative of the presence of QD within the olfactory bulb three hours following aerosolization in mice (data not shown).

TEM images were taken of the glomerular and olfactory nerve layers, where visual microscopy indicated the presence of QD. As can be seen in Fig. 7, QD were broadly dispersed within the axon and occasionally within mitochondria or along the mitochondrial border. Quantum dots were much less common in the olfactory nerve compared to the olfactory bulb. Whereas TEM allows for observation of individual QDs within the olfactory nerve, light microscopy of the whole olfactory bulb shows clusters rather than individual QD given the resolving power of the light microscope.

Microglial cell activation

We differentiated between resting and activated microglial cell morphology as a means of evaluating olfactory bulb responses to particle exposure. Criteria for categorization as ‘resting’ included strong positive staining for RCA-1 and at least two highly branched (ramified) processes extending at least twice the length of a highly elliptical (flattened) nucleus (Fig. 8). Criteria for categorization as ‘activated’ included strong positive staining for RCA-1; not more than two visible processes of more than half the length of the large, roughly circular nucleus; or large overall size and amoeboid shape accompanied by dense staining. Since the intensity and immunological response may be shown in multiple ways, activation of resident (local) microglia and recruitment of additional microglia were considered as independent measures. There was a significantly larger population ($p<0.02$) of activated microglial cells, resident macrophages of the brain, in the glomerular layer of the olfactory bulb in the QD-exposed group than in the sham (Fig. 9). There were no significant differences between exposure groups in the total number of microglial cells observed in the fields counted, a result we interpret as a lack of recruitment.

DISCUSSION

Our primary objective in this study was to demonstrate whether quantum dots (QD) made of coated CdSe/ZnS were transported to the olfactory bulb by axonal transport within olfactory sensory neurons and induced a pro-inflammatory response, indicating toxicity, following a

short-term inhalation exposure. Based on the results, we conclude that following short-term inhalation of solid QD nanoparticles (1 hour), there is rapid (within 3 hours of exposure) olfactory uptake and axonal transport to the brain/olfactory bulb with observed activation of microglial cells, indicating a pro-inflammatory response.

In order for QD to reach the olfactory bulb via nose to brain transport, the particles must first cross the olfactory epithelium. Three different pathways are possible for particles to cross the olfactory epithelium: 1) transcellular, especially across sustentacular cells; 2) paracellular, through tight junctions between sustentacular cells or between sustentacular cells and olfactory neurons; and 3) intracellular, via axonal transport within the olfactory nerve to the glomerular layer of the olfactory bulb where the olfactory axon terminates (Illum 2000, Shepherd 1994). Both fluorescent microscopy and TEM showed QD associated with olfactory nerve and glomerular (terminal to the olfactory nerve) layers of the olfactory bulb, which indicate that QD were taken up by the olfactory sensory neurons and transported by axonal transport to the olfactory bulb. Since QD clusters were observed in the glomerular layer, where particles would exit from the olfactory sensory neurons via axonal transport, and not broadly and uniformly distributed to other areas of the olfactory bulb, we can speculate that QD were most likely transported from the olfactory sensory neurons to the olfactory bulb rather than by other potential pathways (i.e., trigeminal nerve, vascular regions of the nasal cavity, the lungs and systemic transfer from the blood, etc.).

QD appeared to be maintained in a non-aggregated state and transported as single dots to the olfactory bulb, where they formed clusters. This conclusion is based on the following observations: 1) TEM images of aerosol captured by electrostatic precipitation show distinct, single QD particles with PEG2-PE micelles intact; 2) groupings of individual QD, as seen in the micrographs, represent particles captured within a given aerosol droplet and deposited as a cluster on the copper grids; 3) QD were found in the nasal lavage; 4) accumulation of QD was readily detected by fluorescent light microscopy in the glomerular layer of the olfactory bulb, but QD were rarely visualized in the nerve layer and olfactory fascicles traversing the cribriform plate and never as large clusters there; and 5) large clusters were not observed in the electron micrographs of olfactory sensory neuron axons. Since the ability of QD to emit upon excitation with ultraviolet light is a direct function of their crystal lattice structure and size, degradation of structural integrity would manifest as loss of fluorescence or shift in color (Chang et al. 2006). Because there was no loss of fluorescence or a shift in wavelength emitted (and the light observed was the same color as was seen before aerosolization), we can conclude that the QD were transported to and deposited in the olfactory bulb as solid non-degraded particles.

Detection of QD in the olfactory bulb within a few hours after a single one-hour nose only exposure suggests an active mechanism of transport, such as microtubule-mediated axonal transport. Axonal transport can be ‘fast’ or ‘slow’; accepted rates for fast axonal transport are 200–400 mm/day, whereas slow rates are 1–5 mm/day (Shepherd 1994). If we assume an average olfactory epithelium-to-olfactory bulb path distance of 5 mm in the mice, travel time would be 18–36 minutes; ‘slow’ transport would require five days and can be excluded because a greater concentration of QD were observed in the olfactory bulb within a few hours (<3 hours) of inhalation exposure compared to the significantly less amount found in

the olfactory nerve. Only vesicular components are transported via the fast mechanism. Simple diffusion is extremely slow due to the narrowness of the axon, and lateral diffusion along the plasma membrane is even slower. Because the TEM data shows QD inside the axon, we can presumably dismiss simple and lateral diffusion. Therefore, based on the results, we believe that QD undergo fast, vesicle-mediated transport. QD then appear to be able to escape from the olfactory sensory neurons and gain entry to other cells in the olfactory bulb, as evidenced by light micrographs of methacrylate-embedded tissue sections: the images show QD clusters suggestive of lysosomal compartments distributed in the cytoplasm of individual cells within the glomerular layer of the olfactory bulb. From the glomerular layer, QD may have the potential to travel to other areas of the brain (e.g., amygdala, prepyriform cortex, hypothalamus, etc.) as shown with previous studies of other molecules and particles (Illum 2000, Tjalve et al. 1996). On the other hand, studies have shown inability of particles to pass the synapses between the primary and secondary olfactory neurons in the olfactory bulb to the telencephalon and diencephalon (Tjalve et al. 1996). To truly determine this, a longer timeline (i.e., chronic studies with longer post-exposure time) is needed for particles to transport to other areas of the brain (via this pathway).

While no clear evidence of QD exposure-related acute cytotoxicity in either the nasal epithelium or the olfactory bulb was found in this study, increased activation of microglial cells in the olfactory bulbs of mice exposed to QD was observed. There have been many *in vitro* studies demonstrating QD cytotoxicity as demonstrated by altered cell growth, viability and function. Cytotoxicity appears to be dependent on many factors, including QD size, capping materials, color, dose, surface chemistry, coating bioactivity and processing parameters (Jamieson et al. 2007). Much of observed cytotoxicity of QD may be due to the breakdown and release of Cd^{2+} (Chang et al. 2006, Yu et al. 2006). Encapsulation of CdSe with ZnS, as was done here, has previously been shown to reduce free Cd (in the intracellular compartment) and toxicity (Rzigalinski and Strobl 2009). The PEG2-PE QD did not degrade to reveal their active core, yet the presence of solid PEG2-PE QD was enough to elicit a cellular response. This finding suggests QD exiting the olfactory sensory neuron into the extra-cellular space of the olfactory bulb are sufficiently immunogenic to elicit a pro-inflammatory response. Further studies are needed to determine the extent of toxicity and potential neurological effects of QD in the brain.

We chose CdSe cores coated with a layer of ZnS because this chemistry is the most refined. Since the CdSe core is highly reactive and has an unstable structure, coating the core with ZnS increases stability, protects the core from oxidation, prevents leaching of CdSe into the surrounding solution, and produces QD with improved luminescence and higher quantum yields (Jamieson et al. 2007, Medintz et al. 2005). However, capping the core with ZnS alone is not sufficient to stabilize the core in biological solutions; therefore, to render QD more biologically compatible, coatings such as PEG's are used to maintain QD in a non-aggregated state, reduce non-specific adsorption and increase stability and solubility (Jamieson et al. 2007, Rzigalinski and Strobl 2009). We chose to use this technique to ensure that the QD were well dispersed and biologically available.

CONCLUSION

In conclusion, this study demonstrates that when inhaled, QD can undergo nose-to-brain transport via the olfactory sensory neurons. Transport to the olfactory bulb was confirmed by visualizing QD with a variety of microscopy techniques, ranging from fluorescent to transmission electron microscopy, in olfactory axons as well as the olfactory bulb. To observe further potential transport from the glomerular layer to other areas of the olfactory bulb and central nervous system, a longer timeline is needed. The stimulation of a pro-inflammatory response with an increased activation of microglial cells demonstrates the need for further *in vivo* studies via inhalation to determine the extent of toxicity and potential neurological effects of QD in the brain. The study also provides positive findings that solid nanoparticles have the potential to be used for drug delivery and imaging via the nose-to-brain pathway, albeit QD may also display toxic effects once introduced into neural tissues.

Acknowledgments

The authors thank the technical assistance of Dale Uyeminami, Janice Peake and Imelda Espiritu in the aerosolization, fixation and preparation of nasal and olfactory bulb tissue sections for this study. The authors would also like to acknowledge the assistance of researchers Thomas R. Huser and Stephen Lane at the Center for Biophotonics, an NSF Science and Technology Center managed by the University of Calfornia, Davis, under Cooperative Agreement No. PHY 0120999. This work was supported in part by EPA grant RD-83171401, NIEHS grant U01 ES 020127 and NIOSH grant 0H07550 to study the fate and transport of inhaled nanoparticles in the respiratory tract. LEH was supported in part through the Atmospheric Aerosols and Health (AAH) training grant under the UC Statewide Toxic Substances Research and Teaching Program. ESP was supported through training grant number T32HL086350 from the National Heart, Lung, and Blood Institute, NIH.

References

Alivisatos AP, Gu W, Larabell C. Quantum dots as cellular probes. Annu Rev Biomed Eng. 2005; 7:55–76. [PubMed: 16004566]

Aschner M. Nanoparticles: transport across the olfactory epithelium and application to the assessment of brain function in health and disease. Prog Brain Res. 2009; 180:141–152. [PubMed: 20302833]

Bailey RE, Smith AM, Nie S. Quantum dots in biology and medicine. Physica E. 2004; 25:1–12.

Ballou B, Lagerholm BC, Ernst LA, Bruchez MP, Waggoner AS. Noninvasive imaging of quantum dots in mice. Bioconjugate Chemistry. 2004; 15(1):79–86. [PubMed: 14733586]

Chang E, Thekkek N, Yu WW, Colvin VL, Drezek R. Evaluation of quantum dot cytotoxicity based on intracellular uptake. Small. 2006; 2(12):1412–1417. [PubMed: 17192996]

Colton CA, Wilcock DM. Assessing activation states in microglia. CNS Neurol Disord Drug Targets. 2010; 9:174–191. [PubMed: 20205642]

De Lorenzo, AJD. The olfactory neuron and the blood-brain barrier. In: Wolstenholme, GEW.; Knight, J., editors. Ciba Foundation Symposium - Taste and Smell in Vertebrates. Chichester, UK: John Wiley & Sons, Ltd; 1970. p. 151-176.

Dubertret B, Skourides P, Norris DJ, Noireaux V, Brivanlou AH, Libchaber A. In vivo imaging of quantum dots encapsulated in phospholipid micelles. Science. 2002; 298(5599):1759–1762. [PubMed: 12459582]

Elder A, Gelein R, Silva V, Feikert T, Opanashuk L, Carter J, Potter R, Maynard A, Ito Y, Finkelstein J, Oberdorster G. Translocation of inhaled ultrafine manganese oxide particles to the central nervous system. Environ Health Perspect. 2006; 114:1172–1178. [PubMed: 16882521]

Hardman R. A toxicologic review of quantum dots: toxicity depends on physicochemical and environmental factors. Environ Health Perspect. 2006; 114(2):165. [PubMed: 16451849]

Hauke C, Korr H. RCA-I lectin histochemistry after trypsinisation enables the identification of microglial cells in thin paraffin sections of the mouse brain. J Neurosci Methods. 1993; 50:273–277. [PubMed: 7512170]

Hines MA, Guyot-Sionnest P. Synthesis and characterization of strongly luminescing ZnS-capped CdSe nanocrystals. The Journal of Physical Chemistry. 1996; 100(2):468–471.

Illum L. Transport of drugs from the nasal cavity to the central nervous system. Eur J Pharm Sci. 2000; 11:1–18. [PubMed: 10913748]

Jamieson T, Bakhshi R, Petrova D, Pocock R, Imani M, Seifalian AM. Biological applications of quantum dots. Biomaterials. 2007; 28:4717–4732. [PubMed: 17686516]

Kovacs T. Mechanisms of olfactory dysfunction in aging and neurodegenerative disorders. Ageing Res Rev. 2004; 3:215–232. [PubMed: 15177056]

Lawson LJ, Perry VH, Dri P, Gordon S. Heterogeneity in the distribution and morphology of microglia in the normal adult mouse brain. Neuroscience. 1990; 39:151–170. [PubMed: 2089275]

Medintz IL, Uyeda HT, Goldman ER, Mattoussi H. Quantum dot bioconjugates for imaging, labelling and sensing. Nature Materials. 2005; 4(6):435–446.

Oberdorster G, Sharp Z, Atudorei V, Elder A, Gelein R, Kreyling W, Cox C. Translocation of inhaled ultrafine particles to the brain. Inhalation Toxicology. 2004; 16:437–445. [PubMed: 15204759]

Patel S, Chavhan S, Soni H, Babbar AK, Mathur R, Mishra AK, Sawant K. Brain targeting of risperidone-loaded solid lipid nanoparticles by intranasal route. Journal of Drug Targeting. 2011; 19(6):468–474. [PubMed: 20958095]

Raabe OG, Wong TM, Wong GB, Roxburgh JW, Piper SD, Lee JI. Continuous nebulization therapy for asthma with aerosols of beta2 agonists. Ann Allergy Asthma Immunol. 1998; 80:499–508. [PubMed: 9647274]

Rzigalinski BA, Strobl JS. Cadmium-containing nanoparticles: perspectives on pharmacology and toxicology of quantum dots. Toxicology and Applied Pharmacology. 2009; 238(3):280–288. [PubMed: 19379767]

Shepherd, GM. Neurobiology. New York: Oxford University Press; 1994.

Stence N, Waite M, Dailey ME. Dynamics of microglial activation: a confocal time-lapse analysis in hippocampal slices. Glia. 2001; 33:256–266. [PubMed: 11241743]

Tjalve H, Henriksson J, Tallkvist J, Larsson BS, Lindquist NG. Uptake of manganese and cadmium from the nasal mucosa into the central nervous system via olfactory pathways in rats. Pharmacology and Toxicology. 1996; 79(6):347–356. [PubMed: 9000264]

Yu WW, Chang E, Drezek R, Colvin VL. Water-soluble quantum dots for biomedical applications. Biochemical and biophysical research communications. 2006; 348(3):781–786. [PubMed: 16904647]

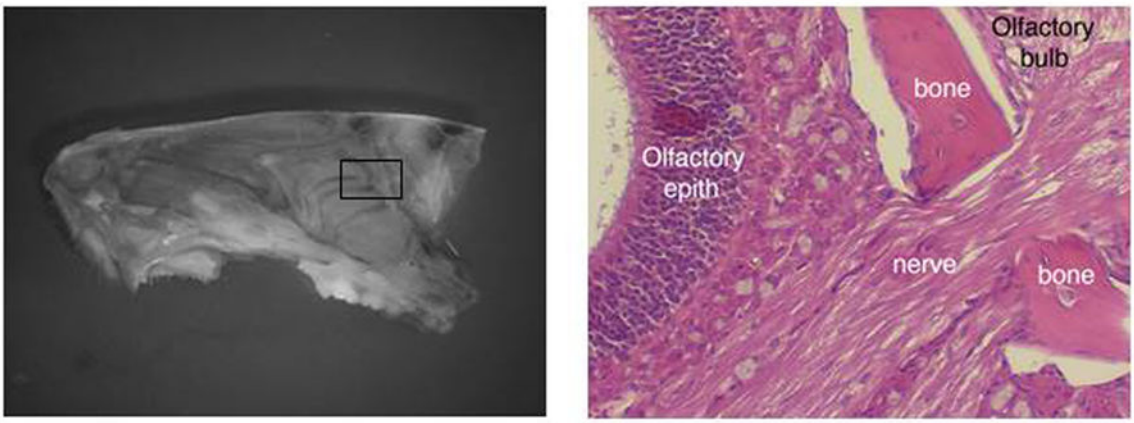

Figure 1.

Left panel, sagittal view of the mouse nasal cavity. Box identifies that region of the nasal cavity sampled for histological analysis shown in the right panel. Right panel, light micrograph of the nose-to-brain pathway showing the olfactory epithelium with nerve fascicles passing through the cribiform plate (space between bony structures) to the olfactory bulb. Tissues have been stained with hematoxylin and eosin. Cross-sectional levels of the nasal cavity and olfactory epithelium showed a lack of any histological evidence for injury (i.e., inflammation or cellular toxicity) based on microscopic evaluation after tissues were stained with hematoxylin and eosin.

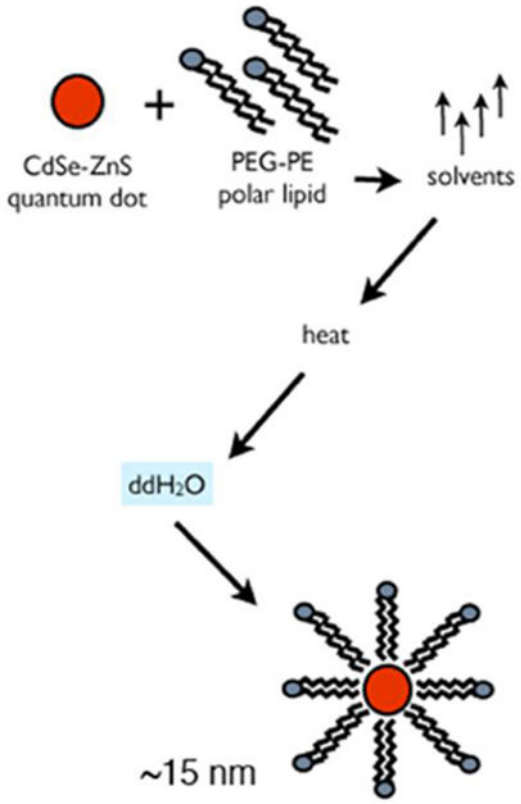

Figure 2.

Quantum dot encapsulation. Cartoon schematic of the technique developed by Dubertret et al. (2002) in which numerous PEG2-PE molecules form a self-assembling micelle around a quantum dot.

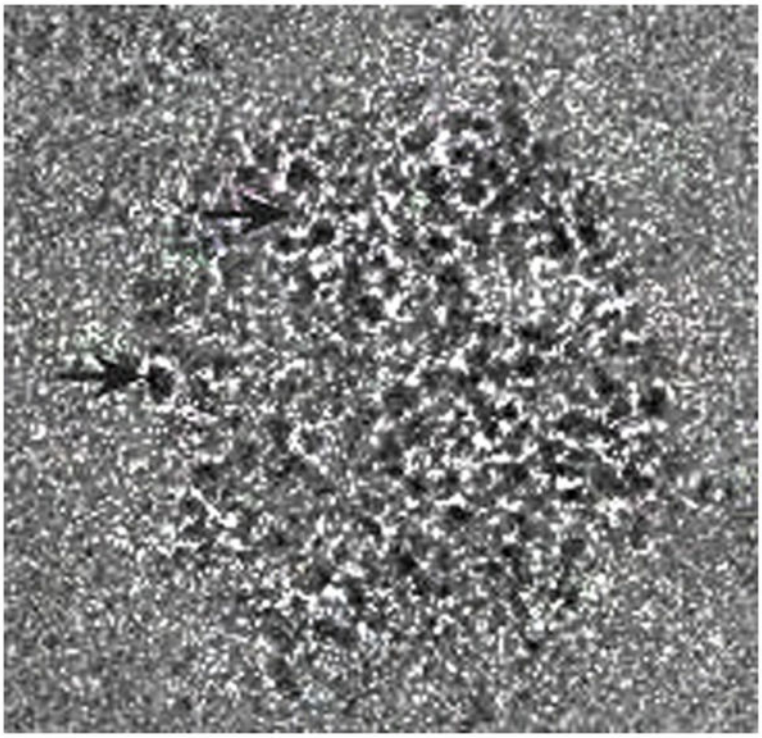

Figure 3.

TEM of a single quantum dot aerosol droplet in which dozens of individual PEG2-PE micelles containing quantum dots can be seen. Arrows indicate good examples of the “bulls eye” effect created by encapsulation.

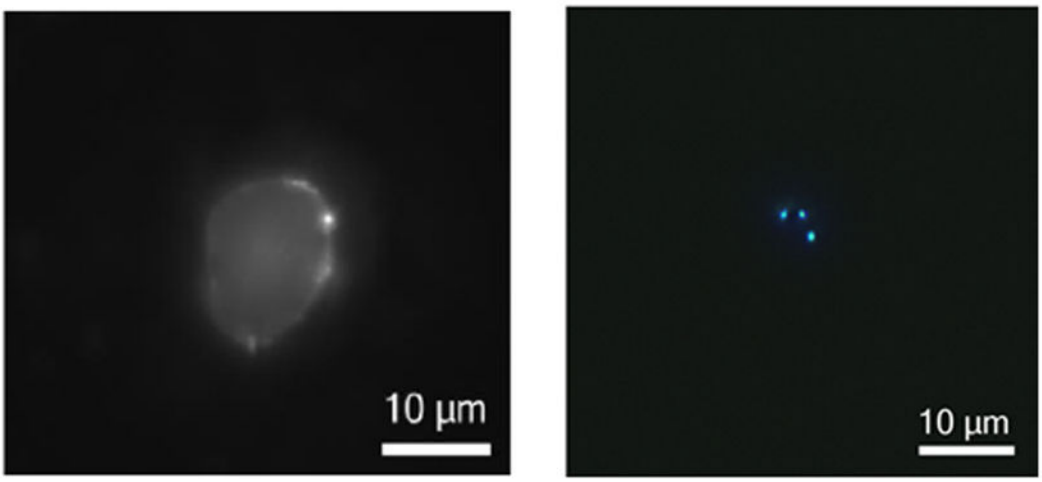

Figure 4.

Left, fluorescent light micrograph of dissociated olfactory bulb tissue from quantum dot aerosol exposed mice with quantum dots at the cell surfaces of intact cells (black and white camera). Right, fluorescent light micrograph of olfactory bulb digests captured with a color camera, of 1.9 nm core (blue) quantum dots.

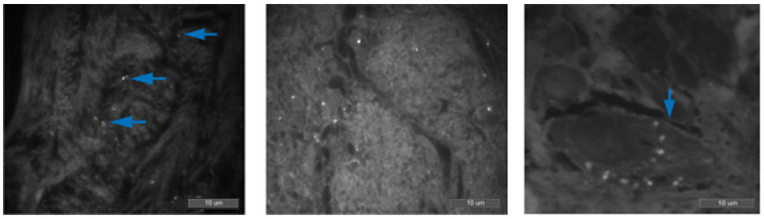

Figure 5.

Fluorescent light micrographs (black and white camera) of methacrylate embedded olfactory bulb tissue. Left, olfactory bulb, olfactory nerve layer. Middle and right, olfactory bulb, glomerular layer. Arrows indicate quantum dots.

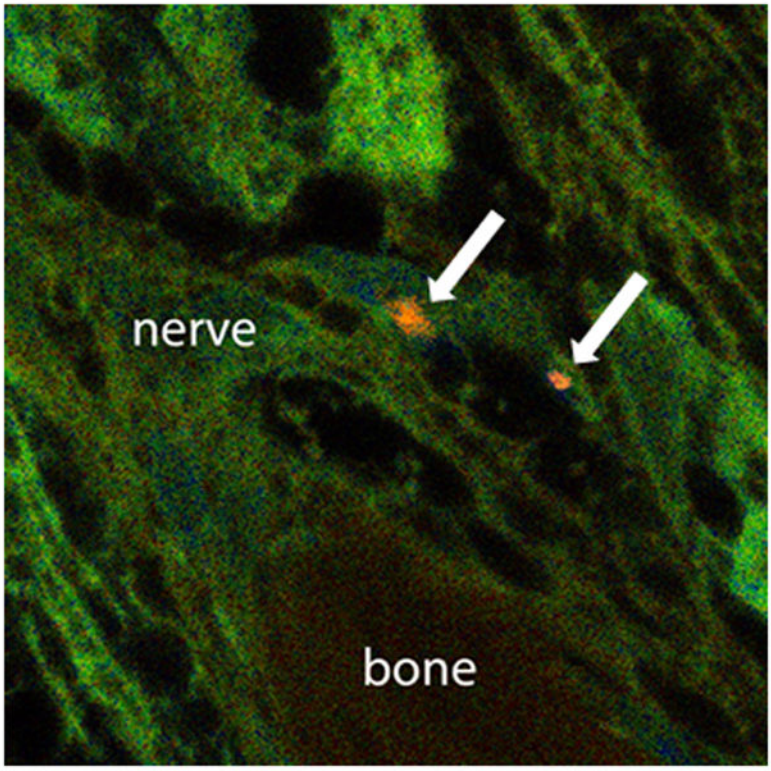

Figure 6.

Energy excitation-loss fluorescence detection of quantum dots in paraffin-embedded nasal tissues. This micrograph illustrates a low level of diffuse false-color imaging of excitation-loss regions within the nerve fascicles passing through the cribiform plate of the cranium. Two small aggregates of more intense aggregation of quantum dots (orange) are shown (arrows). TEM images showed the majority of quantum dots to be within axons. Therefore, quantum dot aggregates are most likely within axons; however, the possibility exists of a periaxonal location as well.

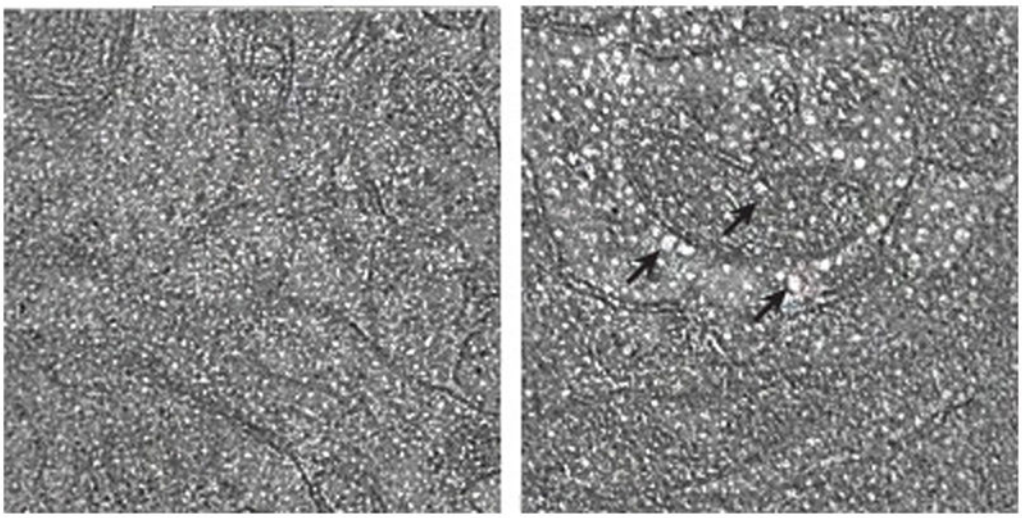

Figure 7.

TEM image of olfactory bulb axon stained with uranyl acetate. Left, sham-exposed animal; Right, quantum dot aerosol-exposed animal. Arrows indicate quantum dots in an olfactory neuron (original magnification 15,000x).

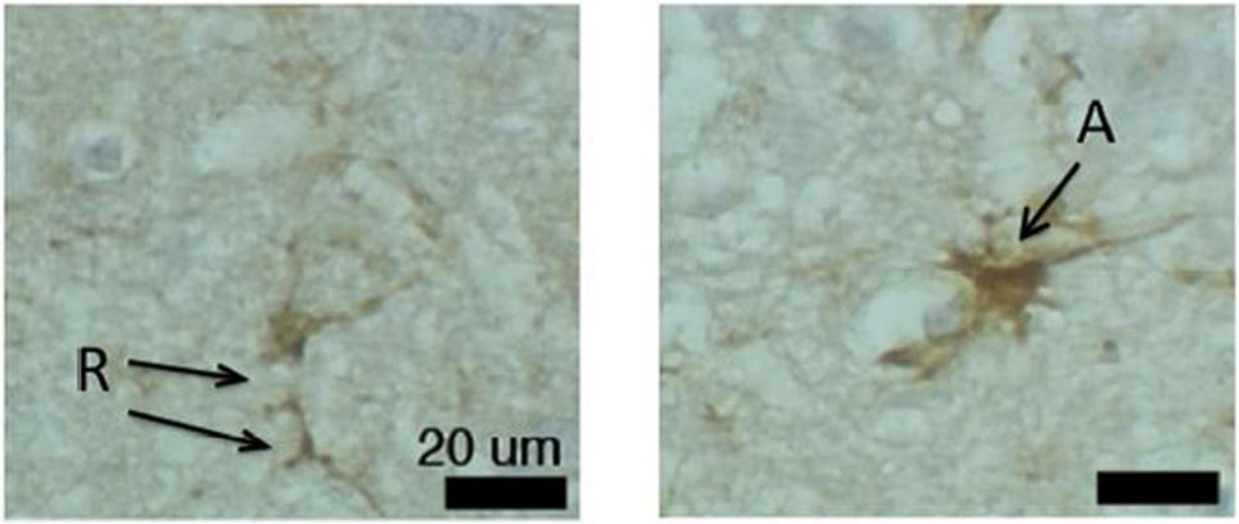

Figure 8.

Light micrographs of paraffin sections of mouse olfactory bulb in which microglial cells are stained brown with RCA-1 lectin + DAB labeling (hematoxylin counterstain). R, microglial cell exhibiting typical non-activated or “resting” morphology with long, highly branched (ramified) processes and a small cellular body; A, microglial cell exhibiting morphology typical of activated state with a large overall size and amoeboid shape.

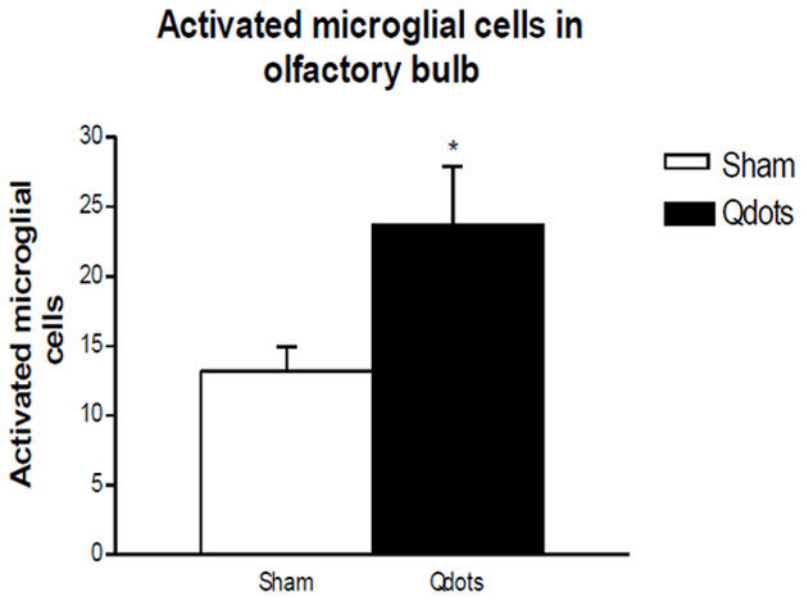

Figure 9.

Comparison of group mean activated microglial cell counts in olfactory bulb. Qualified cells were counted in six fields per section, two sections per animal, six animals per exposure group. *, $p < 0.02$.